ACS APPLIED MATERIALS & INTERFACES

Research Article

www.acsami.org

Fast and Enhanced Broadband Photoresponse of a ZnO Nanowire Array/Reduced Graphene Oxide Film Hybrid Photodetector from the Visible to the Near-Infrared Range

Hao Liu,*[,†] Qi Sun,[‡,§] Jie Xing,[†] Zhiyuan Zheng,[†] Zhili Zhang,[†] Zhiqing Lü,[‡,§] and Kun Zhao*[,‡,§]

[†]School of Science, China University of Geosciences, Beijing 100083, China

[‡]Beijing Key Laboratory of Optical Detection Technology for Oil and Gas, China University of Petroleum, Beijing 102249, China

[§]Key Laboratory of Oil and Gas Terahertz Spectroscopy and Photoelectric Detection, China Petroleum and Chemical Industry Federation (CPCIF), Beijing 100723, China

Supporting Information

ABSTRACT: In the present work, a ZnO nanowire array/reduced graphene oxide film hybrid nanostructure was realized, and the photovoltaic responses from the visible to the near-infrared range were investigated. Compared with the pure ZnO nanowire array and rGO thin film, the hybrid composite exhibited a fast and greatly enhanced broadband photovoltaic response that resulted from the formation of interfacial Schottky junctions between ZnO and rGO.

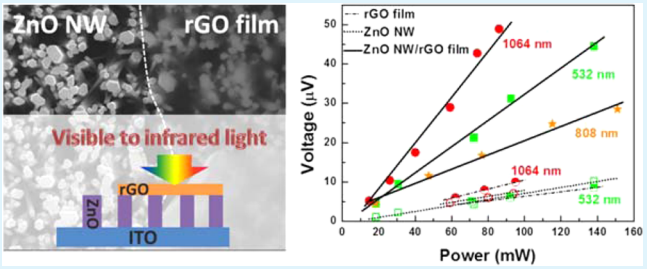

KEYWORDS: *zinc oxide, reduced graphene oxide, nanowire, Schottky junction, photovoltage*

INTRODUCTION

Nanostructured materials with tailored geometries on the nanoscale and tunable nanostructured properties are greatly attractive for photodetection applications.[1−3] This state-of-the-art research primarily focuses on nanostructured metal/metal oxides, such as Au,[4] ZnO,[5] CdS,[6] and nanostructured Si.[7] Among these materials, ZnO has drawn great attention because of its direct wide band gap (∼3.3 eV), large exciton binding energy (∼60 meV), environmentally friendly features, and strong resistance to high-energy proton irradiation. Therefore, many previous studies have fabricated and investigated ZnO-based nanostructured photodetectors.[5,8−11] Nevertheless, most of these photodetectors could work only under the illumination of ultraviolet (UV) light because of the wide band gap of the ZnO material. To develop ZnO-based photodetectors, several strategies have been proposed, including atomic doping[9,12] and the generation of hybrid composites,[13] to extend their photoresponse from the UV to the visible region. However, the device performances, particularly their photoresponsivity and/or response times, have not been satisfactory. For example, the response time of ZnO-based nanostructured photodetectors is usually in the range of seconds to minutes.[8,11,14,15]

One effective way to shorten the response time is by making heterojunctions, such as p−n or Schottky junctions, in ZnO-based devices, which can introduce a built-in electric field to aid in the separation and transport of photocarriers.[16]

Graphene, a two-dimensional (2D) sheet consisting of a single layer of carbon atoms arranged in honeycomb lattice, has drawn great interest because of its remarkable properties, such as a high surface area and high electron mobility.[17] Therefore, applications for graphene have been widely explored in a variety of fields, such as electronics, sensors, catalysis, and energy-related systems.[18,19] Recently, a unique photonic property of graphene has been found, namely, that it can absorb a number of photons from at least the visible to the infrared range even though it is only a single atomic layer thick,[20] which has triggered significant development of graphene-based photodetectors.[21−25] However, the difficulty in synthesizing large-scale graphene with high quality and complexity for making prototype devices has inhibited the application of graphene in optoelectronic devices.[17,19] Conversely, using graphene oxide (GO) as a precursor offers the potential for cost-effective, large-scale production of graphene-based materials.[19] Several photodetectors based on reduced graphene oxide (rGO)[26,27] or rGO-metal oxide (e.g., ZnO) hybrid nanostructures[28−30] have been reported. Nevertheless, these studies have primarily focused on UV photoresponsive behavior. Investigations of the photoresponsive properties in the visible and infrared regions are rare.[30]

Herein, we report a hybrid optoelectronic device based on ZnO nanowires (NW) and an rGO thin film (ZnO NW/rGO film) realized by a simple and inexpensive electrophoretic method. This hybrid sample shows a distinctive rectifying behavior due to the formation of Schottky junctions between ZnO and rGO. We mainly explore the photoresponse in the visible to near-infrared range. It was found that the photo-

Received: December 24, 2014
Accepted: March 13, 2015
Published: March 13, 2015

DOI: 10.1021/am509084r
ACS Appl. Mater. Interfaces 2015, 7, 6645−6651

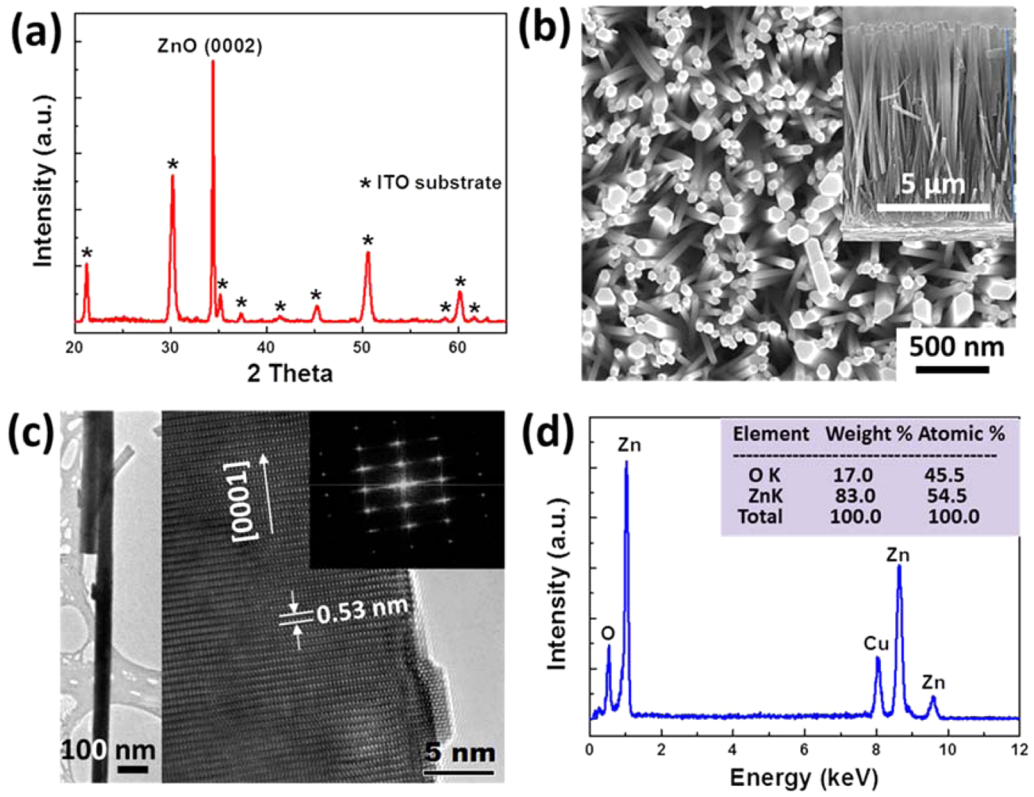

Figure 1. (a) XRD spectrum of ZnO NW arrays grown on an indium tin oxide (ITO) substrate. (b) Top-view SEM image of the ZnO NW arrays. The inset shows the side-view SEM image taken from the same sample. (c) TEM images taken from a single ZnO NW. The inset is the FFT image taken from the HRTEM image. (d) EDX spectrum taken from the same sample.

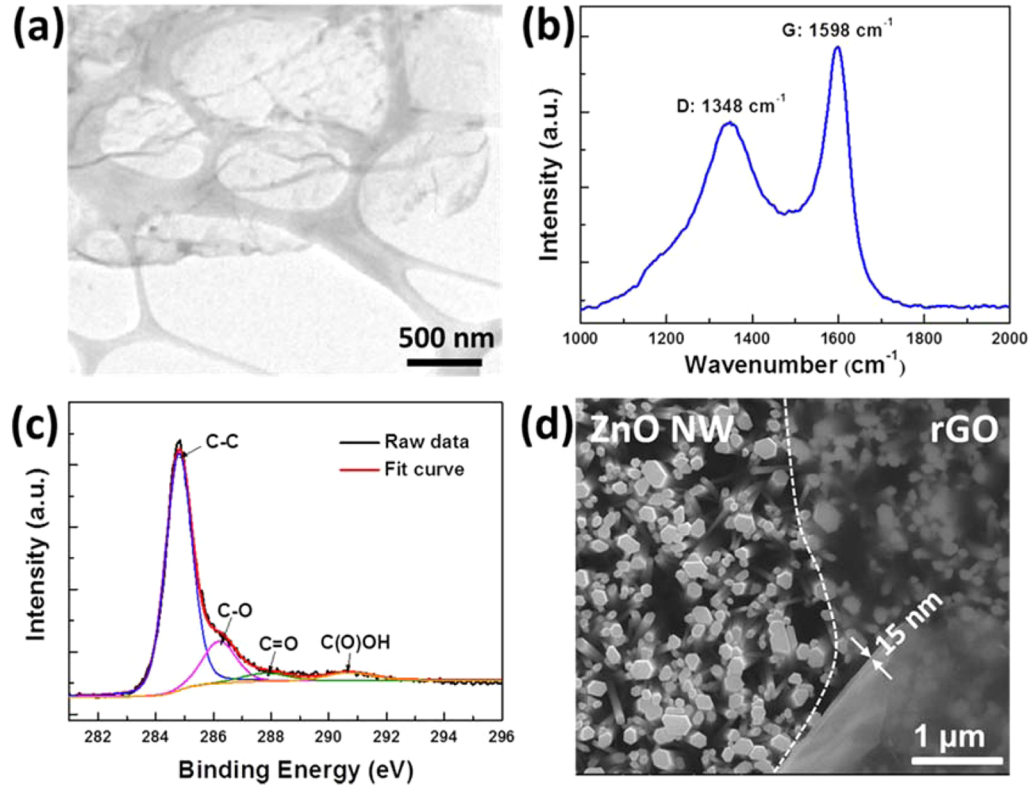

Figure 2. (a) TEM image taken from a typical rGO nanosheet. (b) Raman spectrum of rGO powder. (c) XPS spectra (C 1s) of the same rGO powder. (d) SEM image of the ZnO NW array sample with rGO deposits. The dashed line indicates the boundary of the ZnO and rGO regions.

DOI: 10.1021/am509084r
ACS Appl. Mater. Interfaces 2015, 7, 6645−6651

voltages of the ZnO NW/rGO film hybrid were greatly enhanced with a fast response time (~0.1 s) compared to that of pure ZnO NW arrays and rGO thin film samples. Finally, origins of the enhanced photovoltages are proposed.

RESULTS AND DISCUSSION

The crystal structure of ZnO NW arrays grown on an ITO substrate was examined using X-ray diffraction (XRD), and the patterns are presented in Figure 1a. Only a strong and sharp (0002) diffraction was observed, indicating highly oriented ZnO nanowires (NWs) with good crystalline growth along its crystalline *c*-axis. The other diffraction patterns originated from the ITO substrate. The morphology of the same sample was characterized using field-emission scan electron microscopy (FESEM) and transmission electron microscopy (TEM). In general, the ZnO NWs had well-defined hexagonal-shaped cross sections with diameters of ~60−130 nm (Figure 1b) and lengths of ~8 μm (inset, Figure 1b). The high-resolution TEM (HRTEM) image of a single ZnO NW revealed its lattice structure (Figure 1c). The measured *d*-spacing of the lattices was ~0.53 nm, corresponding to the (0002) plane of wurtzite hexagonal ZnO. In addition, the ZnO NW grew along its crystalline [0001] direction to form a single crystal, as suggested by the fast Fourier transform (FFT) image. The above TEM analyses agreed well with the XRD data. Energy-dispersive X-ray spectroscopy (EDX) showed that the NWs were composed of Zn and O elements (Cu signals come from the TEM grids) (Figure 1d). The atomic ratio between Zn and O elements was close to 1.

Figure 2a shows a TEM image of sheet-like rGO. To check the quality of the rGO, we examined it by both Raman spectroscopy and X-ray photoelectron spectroscopy (XPS). The Raman spectrum (Figure 2b) could disclose the graphitization degree of carbon in the rGO sample by measuring the ratio between the D band (located at ~1348 cm^{-1}, which is attributed to disorders and defects in the graphite structure) and the G band (located at ~1598 cm^{-1}, which denotes the presence of graphite carbon). A relatively low D-to-G band ratio (I_D/I_G ~ 0.74) measured from the present sample suggested that rGO had high crystallinity. However, the reduction of GO to rGO could be examined using XPS (Figure 2c). The C 1s peak of rGO could be decomposed into four different peaks centered at 284.8 eV (corresponding to sp^2 C), 286.2 eV (C−O), 287.8 eV (C═O), and 290.7 eV (C(O)OH). The low intensities of the C−O, C═O, and C(O)OH peaks indicated that GO was efficiently reduced by hydrazine. The zeta-potential measurement indicated that the rGO nanosheet was negatively charged (Figure S1, Supporting Information), resulting from the remaining oxygen-containing functional groups.[31] Thus, rGO nanosheets could be deposited on the ZnO NW/ITO anode during the electrophoretic process. After deposition of rGO, the morphology of the ZnO NW arrays was re-examined using SEM, as shown in Figure 2d. We could clearly observe that a thin rGO layer with a thickness of ~15 nm was deposited on top of the ZnO NW arrays.

The electrical current−voltage (I−V) characteristics of the ZnO NW/rGO film hybrid sample (consisting of ITO/ZnO NW/rGO/Ag contact) were first measured under dark conditions and light illumination, and the results are shown in Figure 3. This sample exhibited a distinctive rectifying behavior under dark conditions. In contrast, an approximately linear I−V characteristic (Figure S2, Supporting Information) was observed in the sample without an rGO thin film (consisting of ITO/ZnO NW/Ag contact). Therefore, the rectifying behavior originated from the Schottky junction between the ZnO and rGO, which has also been observed by other groups.[27,28,32] In addition, the current (I) passing through the Schottky barrier under a forward bias (V) could be determined by the thermionic emission of electrons, which can be described by[32,33]

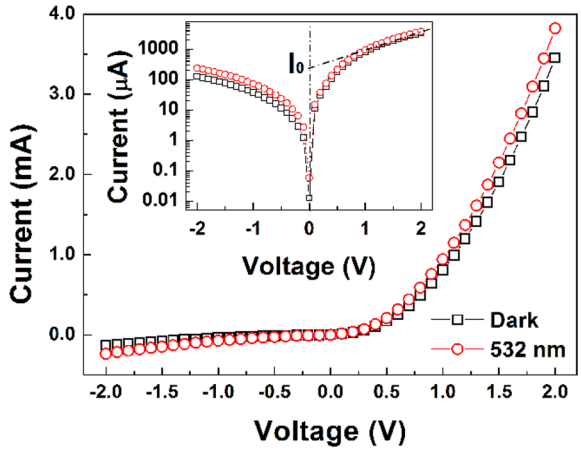

Figure 3. I−V characteristics of the ZnO NW/rGO film hybrid sample in the dark under illumination of a 532 nm laser with a power of ~138 mW. The inset shows a plot of the log current of these characteristics as a function of voltage.

$$I = I_0\left[\exp\left(\frac{qV}{\eta kT}\right) - 1\right], \quad I_0 = AA^*T^2 \exp\left(-\frac{q\Phi_{SB}}{kT}\right)$$

where I_0 is the saturation current, q is the electron charge, η is the ideality factor, k is the Boltzmann constant, T is the absolute temperature, A is the interface area of the Schottky barrier, A^* is the Richardson constant (32 A cm^{-2} K^{-2} for ZnO), and Φ_{SB} is the Schottky barrier height at zero bias. The I_0 value of ~2.25 × 10^{-4} A, which was estimated by extrapolating the I−V curve (inset of Figure 3). Then, the Schottky barrier height Φ_{SB} could be determined as ~0.5 eV.

To investigate the visible to near-infrared light responsive behavior of the ZnO NW/rGO film hybrid detector, we irradiated the sample using continuum solid-state lasers with wavelengths of 532, 808, and 1064 nm. Figure 4 displays the photovoltages of the ZnO NW/rGO film hybrid under irradiation of the 532 nm laser with various energy powers. The response time corresponding to 10−90% of the generated voltage could be extracted from the enlarged Figure 4a. For example, both the rise time (τ_r) and fall time (τ_f) of the photovoltage induced by the 532 nm laser with an energy power of ~138 mW were ~0.1 s, which was much faster than that of most previously reported pure ZnO-based nanostructured photodetectors, which ranged from seconds to minutes.[8,10] The small response time indicated a fast photoresponse characteristic of the ZnO NW/rGO film hybrid. The photovoltaic responsive behavior of this sample under the irradiation of the near-infrared lasers with wavelengths of 808 and 1064 nm was similar to that of Figure 4a. The generated photovoltages of the ZnO NW/rGO film hybrid sample as a function of the energy powers of these three lasers are plotted in Figure 4c. In general, all of the magnitudes of the generated photovoltages increased linearly with the energy powers of the

DOI: 10.1021/am509084r
ACS Appl. Mater. Interfaces 2015, 7, 6645−6651

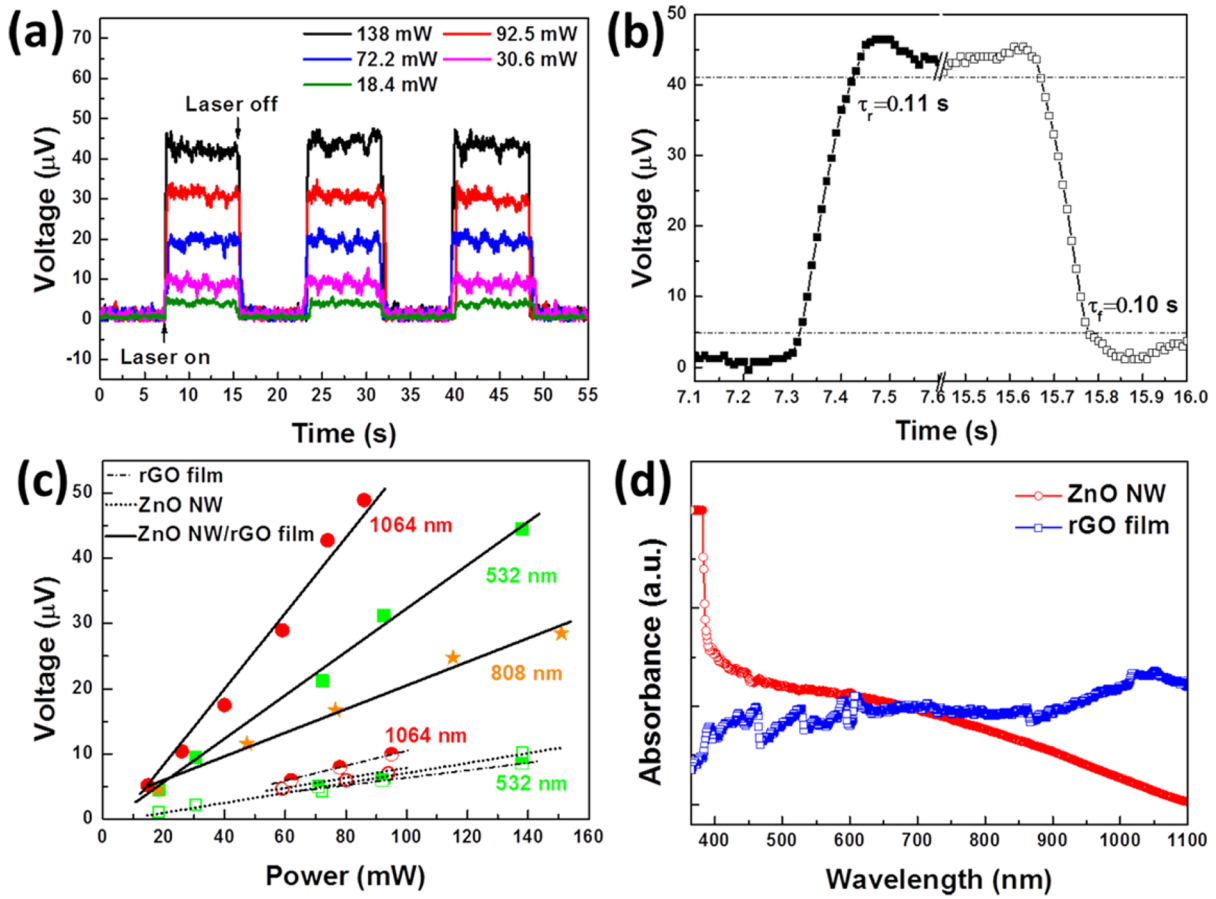

Figure 4. (a) Photovoltaic response of the ZnO NW/rGO film sample under irradiation by a 532 nm He−Ne laser at various powers. (b) Time response of the same sample under irradiation of a 532 nm He−Ne laser with a power of ∼138 mW. (c) The photovoltages of the ZnO NW/rGO film (solid lines), rGO film (dashed dotted line), and ZnO NW (dotted lines) samples as a function of the incident energy power of 532, 808, and 1064 nm lasers. (d) Optical absorption of the ZnO NW arrays and pure rGO samples.

lasers with wavelengths of 532, 808, and 1064 nm. In addition, the ZnO NW/rGO film hybrid sample irradiated with the 1064 nm laser exhibited a photovoltaic responsivity (i.e., photovoltage/on-sample-power) of 0.55 mV/W, which was higher than the other two (0.33 and 0.20 mV/W for the 532 and 808 nm lasers, respectively). To investigate the impact of rGO on the photoresponsive behavior of the ZnO NW/rGO film hybrid sample, we also synthesized and irradiated the other controlled ZnO NW array samples without an rGO layer and a pure rGO thin film sample with the same lasers. Their photovoltages are summarized in Figure 4c, which revealed that the photovoltaic responsivities of the pure ZnO NW arrays under irradiation of 1064 and 532 nm lasers were ∼0.07 mV/W, which was much lower than that of the ZnO NW/rGO film hybrid sample. The photovoltaic response was undetectable when the pure ZnO NW array sample was irradiated with the 808 nm laser. The magnitudes of the photovoltages of the pure rGO thin film were similar to that of the ZnO NW sample, which clearly showed that the photovoltaic response of the ZnO NW/rGO film hybrid sample was significantly enhanced compared with that of pure ZnO NW arrays and the rGO thin film.

To better understand optical properties of the ZnO NW arrays and the pure rGO samples, we tested their optical absorptions, and the results are shown in Figure 4d. The sharp absorption edge near 400 nm of the ZnO NW arrays was attributed to the intrinsic band-edge absorption of the ZnO material. In addition, the results showed a wide absorption in the visible light region due to deep defect energy levels in the ZnO NWs,[34] as revealed by their cathodoluminescence (CL) spectrum (Figure S3, Supporting Information). These defects, including single ionized oxygen vacancies, zinc vacancies, oxygen deficiencies, and so forth, were inherently formed during hydrothermal growth of the ZnO material.[32,34] In the near-infrared region, the optical absorption of the ZnO NW arrays became weak. In contrast, the pure rGO sample showed a wide absorption from the visible to the infrared range, which was consistent with other reports.[20,35]

To better understand the origins of the photovoltages of the ZnO NW/rGO film hybrid, we propose an energy band diagram of this composite as shown in Figure 5. The work functions of ZnO and rGO were ∼4.1 eV[36] and ∼4.9 eV,[37] respectively. When a contact was formed, electrons flowed from ZnO to rGO to achieve thermal equilibrium in the junction until the Fermi levels aligned, resulting in energy band bending. The new energy levels (represented by E_D in Figure 5) in the forbidden gap of ZnO were introduced by deep defects in the ZnO NWs.[34] When the ZnO NW/rGO film hybrid sample was irradiated by visible light, (i.e., the 532 nm laser (∼2.3 eV)), the electrons in the ZnO valence band could be excited to the defect energy levels to form electron−hole pairs. Then, these pairs were separated by the built-in electric field (pointing from ZnO to rGO) induced by the Schottky junction, leading to an increase in the Fermi level of ZnO. In this manner, the

DOI: 10.1021/am509084r
ACS Appl. Mater. Interfaces 2015, 7, 6645−6651

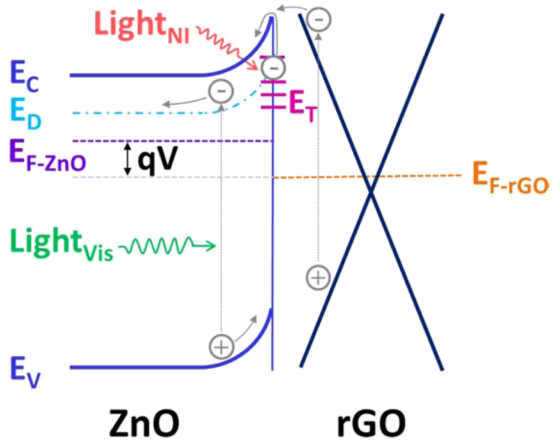

Figure 5. Energy band diagram of the ZnO NW/rGO film hybrid. E_C, E_V, $E_{F\text{-}ZnO}$, E_D, and E_T represent the conduction band, valence band, Fermi level, defect energy levels, and trap level at the interface of the ZnO NWs, respectively. $E_{F\text{-}rGO}$ is the Fermi level of rGO. Light$_{Vis}$ and Light$_{NI}$ represent visible and the near-infrared light, respectively.

photovoltage, (i.e., the potential difference (represented by V in Figure 5) between the Fermi level of ZnO and rGO) was generated. Conversely, the photon energies of the near-infrared light (i.e., the 808 and 1064 nm lasers) were ~1.5 and ~1.2 eV, respectively, which could not directly excite ZnO to generate electron−hole pairs. Nevertheless, O_2 and H_2O molecules were easily absorbed on the surface of nanostructured ZnO by capturing free electrons.[8,38,39] These trapped electrons (represented by E_T in Figure 5) could be excited under infrared light irradiation[40] and drift to ZnO driven by the built-in electric field to generate a photovoltage, upon which the O_2 and H_2O molecules were released. In contrast, when pure ZnO NWs were irradiated with the visible or near-infrared lasers, most generated electrons and holes recombined due to the absence of Schottky junctions, leading to small observed photovoltages (Figure 4c). In addition, a broadband photoresponse from the visible to the mid-infrared range was observed in graphene materials.[20−23,25] Therefore, the electron−hole pairs could be excited in the rGO film from the visible to the near-infrared range and separated by the built-in electric field, which also contributed to the generated photovoltage in the ZnO NW/rGO film hybrid. As a consequence, the photovoltages of the ZnO NW/rGO film hybrid sample from the visible to the infrared regions were significantly enhanced compared to that of the ZnO NW arrays and the pure rGO thin film sample. The higher photovoltaic responsivity under the 1064 nm laser irradiation compared with that of the other two (i.e., the 532 and 808 nm lasers) was consistent with the higher optical absorption of rGO at wavelengths in the 1000−1100 nm region. Furthermore, the photoresponse time of the ZnO NW/rGO film hybrid sample shortened to ~0.1 s (Figure 4b) due to the presence of the interfacial Schottky junctions and the high electronic conductivity of the rGO layer.

CONCLUSIONS

In conclusion, we synthesized a photodetector based on a ZnO NW/rGO film hybrid composite, which was realized by the electrophoretic deposition of rGO on top of ZnO NW arrays. The photovoltages of this photodetector were significantly enhanced from the visible to the near-infrared range compared with that of the pure ZnO NW arrays and the rGO thin film samples, which can be ascribed to the formation of interfacial Schottky junctions at the ZnO NW and rGO interface. The Schottky junctions benefited the separation and transport of the photogenerated carriers. Furthermore, the wide optical absorption of rGO from the visible to the infrared range also contributed to enhancement of the photovoltaic response. We believe that this strategy could be universally applied to a variety of rGO-incorporated nanostructured systems for photodetector applications.

EXPERIMENTAL METHODS

Synthesis of Hydrothermal ZnO NW Arrays. The ZnO NW arrays were synthesized by a hydrothermal method. Briefly, an ITO glass substrate was first wet by 10 mM zinc acetate dihydrate/ethanol solution, and then blown dry with the steam of compressed air. This coating step was repeated five times to get a uniform film on the ITO glass. Then, the substrate was heated to 300 °C to decompose the zinc acetate layer to get a ZnO seed layer on ITO glass. Finally, the ZnO nanowire arrays were synthesized by immersing the coated ITO glass in an aquoues solution containing 25 mM zinc acetate dihydrate (>99%, Sigma) and 25 mM hexamethylenetetramine (>99%, International Laboratory) at 95 °C for 2 h. The hydrothermal process can be repeated several times to get ZnO NWs of a desired length.

Electrophoretic Deposition of rGO on the ZnO NW Arrays. The GO was prepared using a modified Hummers' method[41] followed by reduction by hydrazine in an aqueous solution.[42] The rGO was deposited on the ZnO NW arrays using electrophoresis with a two electrode system in which the ITO glass covered by ZnO NW arrays and Pt foil were employed as anode and cathode, respectively. An external 3 V bias was applied on the ZnO NW/ITO anode for rGO electrophoresis.

Characterizations. The crystallinity of the hydrothermal ZnO NWs were examined by X-ray diffraction (XRD, SmartLab, Rigaku) with a Cu Kα radiation source (d = 0.1541 nm). The morphologies were characterized by FESEM (Quanta 200, FEI). CL was performed at room temperature using a Mono CL system (Oxford Instrument) attached to the FESEM. TEM was also carried out for the microstructural and chemical componential investigation of the samples using a Tecnai F20 microscope equipped with an EDX detector. To characterize the quality of rGO, micro Raman spectrum (RM-1000, Renishaw Co., Ltd.) and XPS (ESCALAB 250, Thermo Fisher Scientific) were performed. The zeta-potential of rGO was measured using a zeta-potential analyzer (Zeta Plus, Brookhaven Instruments Co.). Ultraviolent−visible (UV−vis) absorption spectra were recorded on SP-1702 (Shanghai Spectrum Instrument Co.).

Photoresponse Measurements of the ZnO NW/rGO Film Hybrid and Comparable Samples. For the photovoltaic measurements, the ZnO NW/rGO film hybrid sample was cut into several pieces 1 × 2 cm^2 in size. Two colloidal silver electrodes with 2 × 2 mm^2 were pasted on the surface of the rGO and ITO substrates. Several continuum solid state lasers with wavelengths of 532, 808, and 1064 nm were employed to irradiate the samples in the absence of applied bias at room temperature. The illuminated diameter was limited to 2 mm to avoid exposure of the electrode to the laser. The I−V characteristics of the samples were recorded by a Keithley electrometer. The open-circuit photovoltaic signals were measured by a standard lock-in amplifier technique and recorded by a sampling oscilloscope terminating at 1 MΩ.

ASSOCIATED CONTENT

Supporting Information

Zeta-potential profile of rGO, I−V curve of the ITO/ZnO NW/Ag contact, and CL spectrum of the ZnO nanowires. This material is available free of charge via the Internet at http://pubs.acs.org.

DOI: 10.1021/am509084r
ACS Appl. Mater. Interfaces 2015, 7, 6645−6651

AUTHOR INFORMATION

Corresponding Authors

*E-mail: 2014010007@cugb.edu.cn.

*E-mail: zhk@cup.edu.cn.

Notes

The authors declare no competing financial interest.

ACKNOWLEDGMENTS

This work is supported by the National Natural Science Foundation of China under Grant No. 11104255 and the Fundamental Research Funds for the Central Universities under Grant No. 2011YXL060.

REFERENCES

(1) Konstantatos, G.; Sargent, E. Nanostructured Materials for Photon Detection. *Nat. Nanotechnol.* **2010**, *5*, 391−400.

(2) Zhai, T.; Fang, X.; Liao, M.; Xu, X.; Zeng, H.; Yoshio, B.; Golberg, D. A Comprehensive Review of One-Dimensional Metal-Oxide Nanostructure Photodetectors. *Sensors* **2009**, *9*, 6504−29.

(3) Zhai, T.; Li, L.; Wang, X.; Fang, X.; Bando, Y.; Golberg, D. Recent Developments in One-Dimensional Inorganic Nanostructures for Photodetectors. *Adv. Funct. Mater.* **2010**, *20*, 4233−4248.

(4) Sheldon, M. T.; van de Groep, J.; Brown, A. M.; Polman, A.; Atwater, H. A. Plasmoelectric Potentials in Metal Nanostructures. *Science* **2014**, *346*, 828−831.

(5) Kind, H.; Yan, H.; Messer, B.; Law, M.; Yang, P. Nanowire Ultraviolet Photodetectors and Optical Switches. *Adv. Mater.* **2002**, *14*, 158−160.

(6) Deng, K.; Li, L. CdS Nanoscale Photodetectors. *Adv. Mater.* **2014**, *26*, 2619−2635.

(7) Das, K.; Mukherjee, S.; Manna, S.; Ray, S. K.; Raychaudhuri, A. K. Single Si Nanowire (Diameter ≤ 100 nm) Based Polarization Sensitive Near-Infrared Photodetector with Ultra-High Responsivity. *Nanoscale* **2014**, *6*, 11232−11239.

(8) Soci, C.; Zhang, A.; Xiang, B.; Dayeh, S. A.; Aplin, D. P. R.; Park, J.; Bao, X. Y.; Lo, Y. H.; Wang, D. ZnO Nanowire UV Photodetectors with High Internal Gain. *Nano Lett.* **2007**, *7*, 1003−1009.

(9) Buonsanti, R.; Llordes, A.; Aloni, S.; Helms, B. A.; Milliron, D. J. Tunable Infrared Absorption and Visible Transparency of Colloidal Aluminum-Doped Zinc Oxide Nanocrystals. *Nano Lett.* **2011**, *11*, 4706−4710.

(10) Dai, J.; Xu, C.; Xu, X.; Guo, J.; Li, J.; Zhu, G.; Lin, Y. Single ZnO Microrod Ultraviolet Photodetector with High Photocurrent Gain. *ACS Appl. Mater. Interfaces* **2013**, *5*, 9344−9348.

(11) Zhang, F.; Niu, S.; Guo, W.; Zhu, G.; Liu, Y.; Zhang, X.; Wang, Z. L. Piezo-Phototronic Effect Enhanced Visible/UV Photodetector of a Carbon-Fiber/ZnO-CdS Double-Shell Microwire. *ACS Nano* **2013**, *7*, 4537−4544.

(12) Lin, Y.-G.; Hsu, Y.-K.; Chen, Y.-C.; Chen, L.-C.; Chen, S.-Y.; Chen, K.-H. Visible-Light-Driven Photocatalytic Carbon-Doped Porous ZnO Nanoarchitectures for Solar Water-Splitting. *Nanoscale* **2012**, *4*, 6515−6519.

(13) Ohno, T.; Bai, L.; Hisatomi, T.; Maeda, K.; Domen, K. Photocatalytic Water Splitting Using Modified Gan:ZnO Solid Solution under Visible Light: Long-Time Operation and Regeneration of Activity. *J. Am. Chem. Soc.* **2012**, *134*, 8254−8259.

(14) Hu, L.; Zhu, L.; He, H.; Guo, Y.; Pan, G.; Jiang, J.; Jin, Y.; Sun, L.; Ye, Z. Colloidal Chemically Fabricated ZnO:Cu-Based Photodetector with Extended UV-Visible Detection Waveband. *Nanoscale* **2013**, *5*, 9577−9581.

(15) Li, Y.; Gong, J.; Deng, Y. Hierarchical Structured ZnO Nanorods on ZnO Nanofibers and Their Photoresponse to UV and Visible Lights. *Sens. Actuators, A* **2010**, *158*, 176−182.

(16) Bie, Y.-Q.; Liao, Z.-M.; Zhang, H.-Z.; Li, G.-R.; Ye, Y.; Zhou, Y.-B.; Xu, J.; Qin, Z.-X.; Dai, L.; Yu, D.-P. Self-Powered, Ultrafast, Visible-Blind UV Detection and Optical Logical Operation Based on ZnO/GaN Nanoscale p-n Junctions. *Adv. Mater.* **2011**, *23*, 649−653.

(17) Bonaccorso, F.; Sun, Z.; Hasan, T.; Ferrari, A. C. Graphene Photonics and Optoelectronics. *Nat. Photonics* **2010**, *4*, 611−622.

(18) Chang, H.; Wu, H. Graphene-Based Nanocomposites: Preparation, Functionalization, and Energy and Environmental Applications. *Energy Environ. Sci.* **2013**, *6*, 3483−3507.

(19) Zhu, Y.; Murali, S.; Cai, W.; Li, X.; Suk, J. W.; Potts, J. R.; Ruoff, R. S. Graphene and Graphene Oxide: Synthesis, Properties, and Applications. *Adv. Mater.* **2010**, *22*, 3906−3924.

(20) Nair, R. R.; Blake, P.; Grigorenko, A. N.; Novoselov, K. S.; Booth, T. J.; Stauber, T.; Peres, N. M. R.; Geim, A. K. Fine Structure Constant Defines Visual Transparency of Graphene. *Science* **2008**, *320*, 1308.

(21) Liu, C.-H.; Chang, Y.-C.; Norris, T. B.; Zhong, Z. Graphene Photodetectors with Ultra-Broadband and High Responsivity at Room Temperature. *Nat. Nanotechnol.* **2014**, *9*, 273−278.

(22) Kim, C. O.; Kim, S.; Shin, D. H.; Kang, S. S.; Kim, J. M.; Jang, C. W.; Joo, S. S.; Lee, J. S.; Kim, J. H.; Choi, S.-H.; Hwang, E. High Photoresponsivity in an All-Graphene p−n Vertical Junction Photodetector. *Nat. Commum.* **2014**, *5*, 3429.

(23) Zhang, B.; Liu, T.; Meng, B.; Li, X.; Liang, G.; Hu, X.; Wang, Q. Broadband High Photoresponse from Pure Monolayer Graphene Photodetector. *Nat. Commum.* **2013**, *4*, 1811.

(24) Gan, X.; Shiue, R.-J.; Gao, Y.; Meric, I.; Heinz, T. F.; Shepard, K.; Hone, J.; Assefa, S.; Englund, D. Chip-Integrated Ultrafast Graphene Photodetector with High Responsivity. *Nat. Photonics* **2013**, *7*, 883−887.

(25) Xia, F.; Mueller, T.; Lin, Y.-M.; Valdes-Garcia, A.; Avouris, P. Ultrafast Graphene Photodetector. *Nat. Nanotechnol.* **2009**, *4*, 839−843.

(26) Chitara, B.; Krupanidhi, S. B.; Rao, C. N. R. Solution Processed Reduced Graphene Oxide Ultraviolet Detector. *Appl. Phys. Lett.* **2011**, *99*, 113114.

(27) Chitara, B.; Panchakarla, L. S.; Krupanidhi, S. B.; Rao, C. N. R. Infrared Photodetectors Based on Reduced Graphene Oxide and Graphene Nanoribbons. *Adv. Mater.* **2011**, *23*, 5419−5424.

(28) Shao, D.; Yu, M.; Sun, H.; Hu, T.; lian, J.; Sawyer, S. High Responsivity, Fast Ultraviolet Photodetector Fabricated from ZnO Nanoparticle-Graphene Core-Shell Structures. *Nanoscale* **2013**, *5*, 3664−3667.

(29) Son, D. I.; Yang, H. Y.; Kim, T. W.; Park, W. I. Photoresponse Mechanisms of Ultraviolet Photodetectors Based on Colloidal ZnO Quantum Dot-Graphene Nanocomposites. *Appl. Phys. Lett.* **2013**, *102*, 021105.

(30) Zhan, Z.; Zheng, L.; Pan, Y.; Sun, G.; Li, L. Self-Powered, Visible-Light Photodetector Based on Thermally Reduced Graphene Oxide-ZnO (rGO-ZnO) Hybrid Nanostructure. *J. Mater. Chem.* **2012**, *22*, 2589−2595.

(31) Chavez-Valdez, A.; Shaffer, M. S. P.; Boccaccini, A. R. Applications of Graphene Electrophoretic Deposition. A Review. *J. Phys. Chem. B* **2012**, *117*, 1502−1515.

(32) Nie, B.; Hu, J.-G.; Luo, L.-B.; Xie, C.; Zeng, L.-H.; Lv, P.; Li, F.-Z.; Jie, J.-S.; Feng, M.; Wu, C.-Y.; Yu, Y.-Q.; Yu, S.-H. Monolayer Graphene Film on ZnO Nanorod Array for High-Performance Schottky Junction Ultraviolet Photodetectors. *Small* **2013**, *9*, 2872−2879.

(33) Fu, X.-W.; Liao, Z.-M.; Zhou, Y.-B.; Wu, H.-C.; Bie, Y.-Q.; Xu, J.; Yu, D.-P. Graphene/ZnO Nanowire/Graphene Vertical Structure Based Fast-Response Ultraviolet Photodetector. *Appl. Phys. Lett.* **2012**, *100*, 223114.

(34) Özgür, Ü.; Alivov, Y. I.; Liu, C.; Teke, A.; Reshchikov, M. A.; Doğan, S.; Avrutin, V.; Cho, S.-J.; Morkoç, H. A Comprehensive Review of ZnO Materials and Devices. *J. Appl. Phys.* **2005**, *98*, 041301.

(35) Acik, M.; Lee, G.; Mattevi, C.; Chhowalla, M.; Cho, K.; Chabal, Y. J. Unusual Infrared-Absorption Mechanism in Thermally Reduced Graphene Oxide. *Nat. Mater.* **2010**, *9*, 840−845.

(36) Joondong, K.; Ju-Hyung, Y.; Chang Hyun, K.; Yun Chang, P.; Ju Yeon, W.; Jeunghee, P.; Jung-Ho, L.; Junsin, Y.; Chang-Soo, H. ZnO Nanowire-Embedded Schottky Diode for Effective UV Detection by the Barrier Reduction Effect. *Nanotechnology* **2010**, *21*, 115205.

DOI: 10.1021/am509084r
ACS Appl. Mater. Interfaces 2015, 7, 6645−6651

(37) Kang, B.; Lim, S.; Lee, W. H.; Jo, S. B.; Cho, K. Work-Function-Tuned Reduced Graphene Oxide via Direct Surface Functionalization as Source/Drain Electrodes in Bottom-Contact Organic Transistors. *Adv. Mater.* **2013**, *25*, 5856−5862.
(38) Ghosh, R.; Dutta, M.; Basak, D. Self-Seeded Growth and Ultraviolet Photoresponse Properties of ZnO Nanowire Arrays. *Appl. Phys. Lett.* **2007**, *91*, 073108.
(39) Dai, W.; Yang, Q.; Gu, F.; Tong, L. ZnO Subwavelength Wires for Fast-Response Mid-Infrared Detection. *Opt. Express* **2009**, *17*, 21808−21812.
(40) Liu, H.; Zhao, S.; Zhao, K.; Liu, W. Photovoltaic Responses of ZnO/Si Heterojunctions Synthesized by Sol-Gel Method. *Eur. Phys. J.: Appl. Phys.* **2011**, *55*, 10501.
(41) Marcano, D. C.; Kosynkin, D. V.; Berlin, J. M.; Sinitskii, A.; Sun, Z.; Slesarev, A.; Alemany, L. B.; Lu, W.; Tour, J. M. Improved Synthesis of Graphene Oxide. *ACS Nano* **2010**, *4*, 4806−4814.
(42) Stankovich, S.; Dikin, D. A.; Piner, R. D.; Kohlhaas, K. A.; Kleinhammes, A.; Jia, Y.; Wu, Y.; Nguyen, S. T.; Ruoff, R. S. Synthesis of Graphene-Based Nanosheets via Chemical Reduction of Exfoliated Graphite Oxide. *Carbon* **2007**, *45*, 1558−1565.

DOI: 10.1021/am509084r
ACS Appl. Mater. Interfaces 2015, 7, 6645−6651